Modeling of Particle Growth and Morphology in the Gas Phase Polymerization of Butadiene. I. Model and Its Solution Method

JUNZI ZHAO, JIANZHONG SUN, QIYUN ZHOU, ZUREN PAN

Department of Chemical Engineering, Zhejiang University, Hangzhou 310027, People's Republic of China

Received 9 May 2000; accepted 28 August 2000

ABSTRACT: An improved multigrain model designed to simulate the polymeric particle growth and morphology in the gas phase polymerization of butadiene was developed. In the model, the effects of intraparticle heat and mass transfers, heat and mass transfer resistances at the particle boundary layer, sorption of 1,3-butadiene in 1,4-*cis*-polybutadiene, and intrinsic kinetics on the polymeric particle growth and morphology were considered. An improved numerical method was also proposed. © 2001 John Wiley & Sons, Inc. J Appl Polym Sci 81: 719–729, 2001

Key words: butadiene; gas phase polymerization; modeling; particle growth; morphology

INTRODUCTION

The gas phase polymerization of butadiene by heterogeneous catalysts was studied in recent years.[1,2] Various models at the mesoscale level for the gas phase polymerization of olefins by heterogeneous catalysts have been established. The multigrain model and the multilayer model are two types of models that could describe reasonably well the phenomena that occur at the mesoscale level during polymerization by Ziegler–Natta catalysts.[3–7] Modeling of gas phase polymerization of butadiene in terms of the polymeric multilayer model was proposed by Jianzhong et al.[3] Garmatter et al.[8] studied the polymeric particle growth and morphology of butadiene gas phase polymerization using an online microscopic technique.[8] No reports have been published on modeling of polymeric particle growth and morphology in the gas phase polymerization of butadiene at the mesoscale level using the multigrain model.

The goal of this article is to develop an improved model based on the multigrain model that could be used to simulate the effects of kinetics, heat and mass transfers, and sorption of 1,3-butadiene in 1,4-*cis*-polybutadiene on the polymeric particle growth and morphology in the gas phase polymerization of butadiene by a heterogeneous catalyst. An improved numerical solution technique is also be proposed.

POLYMERIC PARTICLE MODEL

The multigrain model is based on numerous experimental observations that the original catalyst particle quickly breaks up into many small catalyst fragments (primary crystallites) after the beginning of polymerization, which are dispersed throughout the growing polymer particle. Thus, the large macroparticle is composed of many

Correspondence to: J. Sun.

Contract grant sponsor: National Natural Science Foundation of China; Contract grant number: 29876035.

Journal of Applied Polymer Science, Vol. 81, 719–729 (2001)

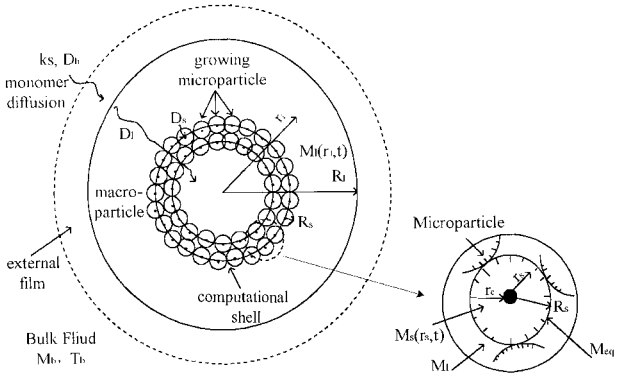

Figure 1 Scheme of the multigrain model.

small polymer particles (microparticles) that encapsulate these catalyst fragments. This idealized picture is represented schematically in Figure 1.[5] For a monomer to reach the active sites, there are two sequential types of diffusion: macrodiffusion (subscript l) in the interstices between the microparticles, and microdiffusion (subscript s) within the microparticles. Figure 2 demonstrates the monomer concentration and temperature gradients in the macroparticle and in the microparticle.

The full set of material and energy balances for the growing polymer particle is presented in Tables I and II. The equations differ from those presented by Floyd et al. and Hutchinson et al.[7] only in notations and some boundary and initial conditions.[5–7] In the derivation of these balances, the following assumptions are made:

1. Catalyst completely breaks up into fragments, which have the same size at time zero.
2. Replication is observed, at both the macroparticle and microparticle level.
3. Particles (micro and macro) are of spherical shape.
4. The active sites are dispersed uniformly in the catalyst particle.
5. Polymer production occurs pseudohomogeneously at the macroparticle scale.

In Table I, R_{cs} is the rate of polymerization at the catalyst particle surface, given by

$$R_{cs} = k_p C^* M_c \tag{1}$$

where k_p is the propagation rate constant, C^* is the concentration of the active sites, and M_c is the monomer concentration at the catalyst surface.

The equations given in Tables I and II must be solved simultaneously to obtain the distribution of the monomer concentration and temperature in the macroparticle and in the microparticle for the simulation of the growth and morphology of the polymeric particle.

NUMERICAL SOLUTION METHOD

Gradients of Monomer Concentration and Temperature in the Microparticle

First, consider the time scale for mass and energy transfers in the microparticle to reach quasi-steady state. The time constant for the monomer concentration to reach a quasi-steady state is given approximately by

$$\tau_{M_s} = \frac{R_s^2}{D_s} \tag{2}$$

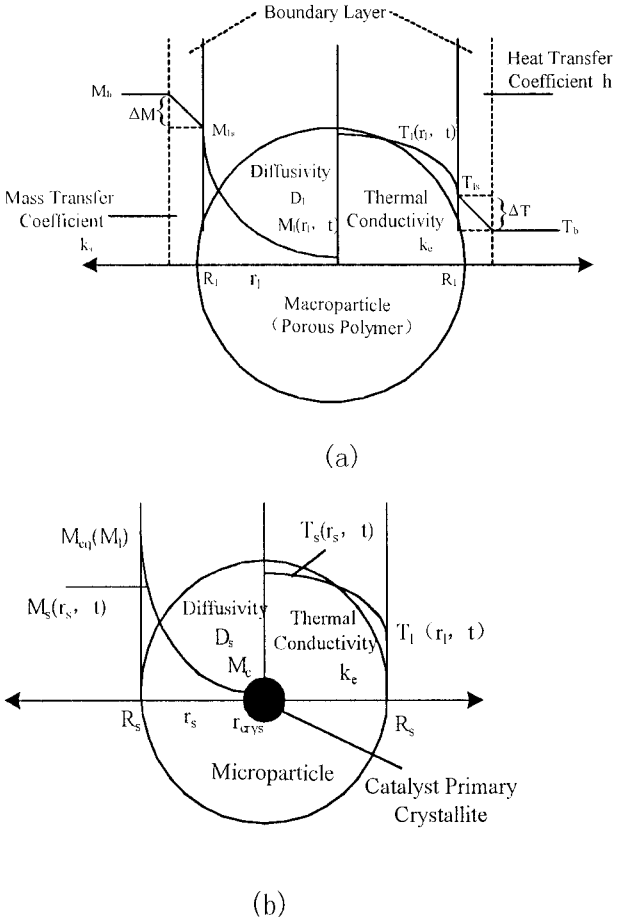

Figure 2 Concentration and temperature gradients in the macroparticle (a) and microparticle (b).

Table I Mass Balances for Macroparticle and Microparticle in the Multigrain Model

Macroparticle ($0 \le r_l \le R_l$)	Microparticle ($r_{\text{crys}} \le r_s \le R_s$)
$\varepsilon_l \dfrac{\partial M_l}{\partial t} = \dfrac{1}{r_l^2}\dfrac{\partial}{\partial r_l}\left(D_l r_l^2 \dfrac{\partial M_l}{\partial r_l}\right) - R_v$	$\dfrac{\partial M_s}{\partial t} = \dfrac{1}{r_s^2}\dfrac{\partial}{\partial r_s}\left(D_s r_s^2 \dfrac{\partial M_s}{\partial r_s}\right)$
B.C.	B.C.
$r_l = 0, \quad \dfrac{\partial M_l}{\partial r_l} = 0$	$r_s = r_{crys}, \; 4\pi r_{crys}^2 D_s \dfrac{\partial M_s}{\partial r_s} = \dfrac{4}{3}\pi r_{crys}^3 R_{cs}$
$r_l = R_l, \quad D_l \dfrac{\partial M_l}{\partial r_l} = k_s(M_b - M_1), \qquad M_l = M_{ls}$	$r_s = R_s, \qquad M_s = M_{eq}(M_l)$
I.C.	I.C.
$t = 0, \qquad R_l = R_c, \qquad M_l = 0$	$t = 0, \qquad R_s = r_{crys}, \qquad M_s = 0$

which yields a time constants τ_{M_s}, a fraction of a second for reasonable values of R_s, D_s (i.e., $10^{-6} \le R_s \le 10^{-4}$ cm, $1.94 \le D_s \le 47.81 \times 10^{-8}$ cm^2/s). Similarly, the approximate time scale for temperature equilibrium in the microparticle may be expressed as

$$\tau_{T_s} = \frac{R_s^2 C_p \rho_p}{k_e} \tag{3}$$

which gives a thermal time constant of, at most, a fraction of a second for reasonable values of R_s, ρ_p, C_p and k_e (ρ_p = 890 kg/m^3, C_p = 1600 J/kg K, k_e = 0.11 W/m K). Considering that the time scale for particle growth is on the order of hours, it may be assumed that the quasi-steady state approximation (QSSA) is valid for both the monomer concentration and temperature in the microparticle.

Using the QSSA with the mass and energy balances for the microparticle, the monomer concentration and temperature at the catalyst surface can be obtained as

$$M_c = \frac{M_{\text{eq}}(M_l)}{1 + \frac{1}{3}\alpha_s^2(\phi_s - 1)/\phi_s} \tag{4}$$

$$T_c = T_l + \frac{\frac{1}{3}\beta_s \, \alpha_s^2(\phi_s - 1)/\phi_s}{1 + \frac{1}{3}\alpha_s^2(\phi_s - 1)/\phi_s} M_{\text{eq}}(M_l) \tag{5}$$

where α_s is a Thiele modulus, $\alpha_s = r_c(k_p C^*/D_s)^{1/2}$, $\beta_s = (-\Delta H_p)D_s/k_s$, and $\phi_s = R_s/r_c$ is the microparticle growth factor.

Equations (4) and (5) can be combined to yield a relation between the temperature and concentration gradients

Table II Energy Balances for Macroparticle and Microparticle in the Multigrain Model

Macroparticle ($0 \le r_l \le R_l$)	Microparticle ($r_{crys} \le r_s \le R_s$)
$\dfrac{\partial T_l}{\partial t} = \dfrac{1}{r_l^2}\dfrac{\partial}{\partial r_l}\left(\dfrac{k_e}{C_p\rho_p} r_l^2 \dfrac{\partial T_l}{\partial r_l}\right) + \dfrac{(-\Delta H_p)}{C_p\rho_p} R_v$	$\dfrac{\partial T_s}{\partial t} = \dfrac{1}{r_s^2}\dfrac{\partial}{\partial r_s}\left(\dfrac{k_e}{C_p\rho_p} r_s^2 \dfrac{\partial T_s}{\partial r_s}\right)$
B.C.	B.C.
$r_l = 0, \qquad \dfrac{\partial T_l}{\partial r_l} = 0$	$r_s = r_{crys}$
$r_l = R_l, \qquad k_e \dfrac{\partial T_l}{\partial r_l} = h(T_b - T_l)$	$-4\pi r_{\text{crys}}^2 k_e \dfrac{\partial T_s}{\partial r_s} = \dfrac{4}{3}\pi r_{\text{crys}}^3 R_{\text{cs}}(-\Delta H_p)$
	$r_s = R_s, \qquad T_s = T_l$
I.C.	I.C.
$t = 0, \qquad T_l = T_b$	$t = 0, \qquad T_s = T_b$

$$T_c - T_l = \frac{(-\Delta H_p)D_s[M_{\text{eq}}(M_l) - M_c]}{k_e} = \beta_s[M_{\text{eq}}(M_l) - M_c)] \quad (6)$$

Equation (6) will give a maximal possible temperature rise in the microparticle. Using the relative parameter values, the maximal temperature rise in the microparticles is found to be a fraction of a degree. Thus, there is always a negligible intraparticle temperature rise in the microparticle for the gas phase polymerization of butadiene. This conclusion is independent of catalyst activity, catalyst primary crystallite size, and other such factors. It is also identical to the case in the polymerization of olefins.[5]

Thus, the microparticle mass balance may be simplified into a simple algebraic equation, and the microparticle energy balance is eliminated from the overall calculation.

Volume Balance Over Microparticle

The volume balance over the microparticle can be given by

$$\frac{dV_s}{dt} = 4\pi R_s^2 \frac{dR_s}{dt} = \frac{4}{3}\pi r_{\text{crys}}^3 k_p C^*(t) M_c(t) MW/\rho_p \quad (7)$$

$$\phi_s^3(t_2) = \phi_s^3(t_1) + \frac{k_p MW}{\rho_p}\int_{t_1}^{t_2} M_c(t)C^*(t)\, dt \quad (8)$$

if the time interval $t_2 - t_1$ is small enough, $\phi_s(t_2)$ can be calculated approximately by

$$\phi_s(t_2) = \left(\phi_s^3(t_1) + \left[\frac{k_p MW(t_2 - t_1)}{\rho_p}\right] \times \left\{\frac{[M_c(t_1)C^*(t_1) + M_c(t_2)C^*(t_2)]}{2}\right\}\right)^{1/3} \quad (9)$$

Practical simulations indicate that a very small time step is necessary to track the rapid change in the particle size at the early time, and satisfactory results can be obtained by iteration calculations. Later in the particle lifetime, much larger steps can be taken without loss of accuracy.

Discretization of the Model Equations

As shown in Figure 3, the particle is divided into N concentric shells at time zero, with each shell of equal thickness. At the beginning of the reaction, the concentration of the active sites in each shell is the same. There are no active sites and support at the boundaries of each shell (i.e., at each node). The temperature and monomer concentration are uniform in each shell and can be expressed as the arithmetic averages at the two relevant neighboring nodes. The discretization is implemented mainly by the 3-point Lagrangian interpolating polynominal.

It is observed experimentally that polymer of low bulk density is often produced at high rates of polymerization, but significantly higher bulk densities can result by adding a prepolymerization step. Hutchinson et al.[7] considered that poor particle morphology may be attributable to high intraparticle void fraction resulting from uneven rates of growth within the polymer macroparticle. It is one of the goals of this study to examine the effect of uneven growth rates on particle morphology.

Diffusivity within the macroparticle is assumed to be proportional to void fraction of the macroparticle according to the expression[5,7]

$$D_l = \frac{\varepsilon_l D_b}{\tau} \quad (10)$$

Thus, the mass balance for the macroparticle is expanded into

$$\varepsilon_l \frac{\partial M_l}{\partial t} = \frac{D_b}{\tau}\left(\varepsilon_l \frac{2}{r_l}\frac{\partial M_l}{\partial r_l} + \varepsilon_l \frac{\partial^2 M_l}{\partial t^2} + \frac{\partial \varepsilon_l}{\partial r_l}\frac{\partial M_l}{\partial r_l}\right) - R_v \quad (11)$$

The various terms in eq. (11) are discretized according to the following expressions:

$$\varepsilon_l|_{r_l(j)} = \tfrac{1}{2}[\varepsilon_l(j) + \varepsilon_l(j+1)] \qquad j = 1, 2 \cdots N-1 \quad (12)$$

$$\left.\frac{\partial \varepsilon_l}{\partial r_l}\right|_{r_l(j)} = \frac{[\varepsilon_l(j+1) - \varepsilon_l(j)]}{[r_l(j+1) + r_l(j-1)]/2} \qquad j = 1, 2 \cdots N-1 \quad (13)$$

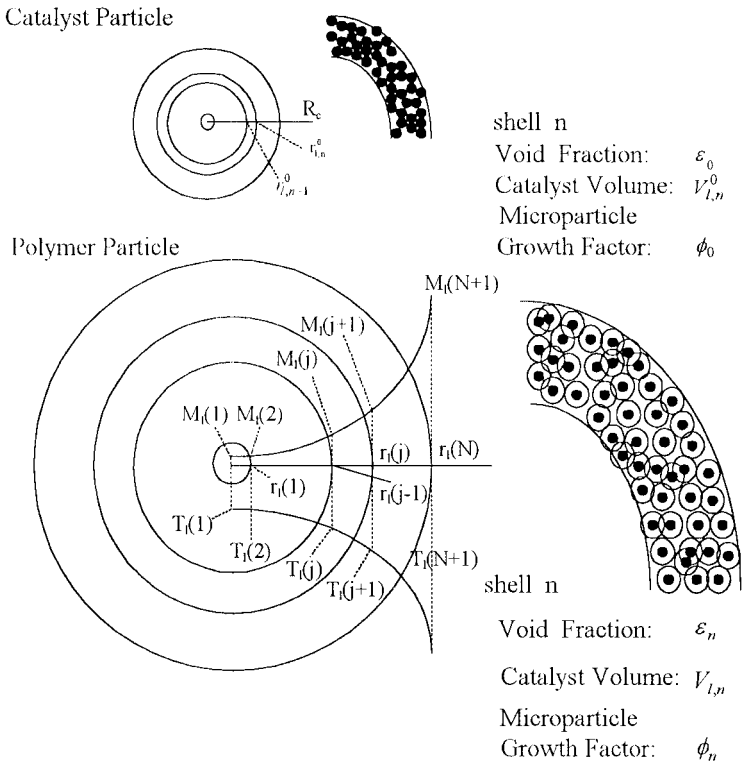

Figure 3 Scheme of discretization and tracking of particle growth in the multigrain model.

$$\left.\frac{\partial M_l}{\partial r_l}\right|_{r_l(j)} = \frac{r_l(j) - r_l(j+1)}{[r_l(j-1) - r_l(j)] \times [r_l(j-1) - r_l(j+1)]} M_l(j) + \frac{2r_l(j) - r_l(j-1) - r_l(j+1)}{[r_l(j) - r_l(j-1)] \times [r_l(j) - r_l(j+1)]} M_l(j+1) + \frac{r_l(j) - r_l(j-1)}{[r_l(j+1) - r_l(j-1)] \times [r_l(j+1) - r_l(j)]} M_l(j+2)$$

$$j = 2, 3 \cdots N-1 \tag{14}$$

$$\left.\frac{\partial^2 M_l}{\partial r_l^2}\right|_{r_l(j)} = \frac{2M_l(j)}{[r_l(j-1) - r_l(j)] \times [r_l(j-1) - r_l(j+1)]} + \frac{2M_l(j+1)}{[r_l(j) - r_l(j-1)][r_l(j) - r_l(j+1)]} + \frac{2M_l(j+2)}{[r_l(j+1) - r_l(j-1)] \times [r_l(j+1) - r_l(j)]}$$

$$j = 2, 3 \cdots N-1 \tag{15}$$

With respect to $j = 1$, $r_l(j-1) = 0$, $r_l(j) = r_l(1)$, $r_l(j+1) = r_l(2)$. Substituting 0, $r_l(1)$, $r_l(2)$ for $r_l(j-1)$, $r_l(j)$, $r_l(j+1)$ in eqs. (14) and (15), respectively, can result in

$$\left.\frac{\partial M_l}{\partial r_l}\right|_{r_l(1)} \quad \text{and} \quad \left.\frac{\partial^2 M_l}{\partial r_l^2}\right|_{r_l(1)}$$

Discretization of Eq. (11) at the Particle Center that Corresponds to j = 0

According to the boundary condition,

$$r_l = 0, \qquad \frac{\partial M_l}{\partial r_l} = \frac{\partial \varepsilon_l}{\partial r_l} = 0$$

and the well-known theorem

$$\lim_{x\to 0} \frac{1}{x}\frac{\partial y}{\partial x} = \frac{\partial^2 y}{\partial x^2},$$

the following expressions can be obtained:

$$\varepsilon_l \left.\frac{\partial M_l}{\partial t}\right|_{r_l(0)} = \frac{6D_b\varepsilon_l}{\tau}\frac{1}{r_l^2(1)}[M_l(2) - M_l(1)] - R_v \tag{16}$$

Discretization of Eq. (11) on the external boundary corresponding to j = N

To maintain the same accuracy with the interior points, eq. (11) is discretized on the external boundary also through 3-point interpolating polynominal, while the term $M_l(N-1)$ is managed to be eliminated from the resulting expressions. Using the relevant boundary condition, the mass balance on the external boundary can be discretized into

$$\begin{aligned}\left.\frac{\partial M_l}{\partial t}\right|_{r_l(N)} = {} & \frac{D_b}{\tau}\frac{2}{[r_l(N) - r_l(N-1)]^2}M_l(N) - \left[\frac{D_b}{\tau}\frac{2}{[r_l(N) - r_l(N-1)]^2} + \frac{2k_s}{\varepsilon_l[N](r_l(N) - r_l(N-1)]}\right. \\ & \left. + \frac{2k_s}{r_l(N)\varepsilon_l(N)} + \frac{\varepsilon_l(N) - \varepsilon_l(N-1)}{\varepsilon_l(N)^2}\frac{2k_s}{[r_l(N) + r_l(N-1)]}\right] M_l(N+1) \\ & + \left[\frac{2k_s}{r_l(N)\varepsilon_l(N)} + \frac{2k_s}{\varepsilon_l(N)[r_l(N) - r_l(N-1)]} + \frac{\varepsilon_l(N) - \varepsilon_l(N-1)}{\varepsilon_l^2(N)}\frac{2k_s}{[r_l(N) + r_l(N-1)]}\right]M_b - \frac{R_v}{\varepsilon_l(N)}\end{aligned} \tag{17}$$

In the above equations, the macroparticle volumetric rate of monomer consumption, R_v, has units of (mol monomer/L s) and is related to the monomer consumption rate in the microparticle according to the expression

$$R_v = k_p M_c C^*(1 - \varepsilon_l)/\phi_s^3 \tag{18}$$

where ε_l is the local macroparticle void fraction. This expression illustrates the dilution effect caused by polymer formation within the macroparticle. As the microparticle increases in size, the macroparticle volumetric rate of polymerization decreases. Thus, the most severe transfer limitations in the macroparticle occur early in the particle lifetime. This also indicates that very small time step is required at the beginning of polymerization.

As for the discretization of $(\partial M_l)/(\partial t)$, it is generally hypothesized that the QSSA is valid for the mass transfer in the macroparticle (i.e., $(\partial M_l)/(\partial t) = 0$.[4] But the practical simulations indicated that in such cases as the catalyst activity is high, the catalyst diameter is large, D_l is low, and so on, which imply that the mass transfer limitations may be severe, the program collapsed in a short time. Thus, the discretization of $(\partial M_l)/(\partial t)$ and the updating of grid must be implemented in the following way:

$$\frac{\partial M_l}{\partial t} = \frac{M_l(j, k+1) - M_l(j, k)}{\Delta t} \tag{19}$$

The idea of eq. (19) requires that the calculation of the profiles of monomer concentration be finished before the grid is updated from the mathematical point. In this case, the overall rate of polymerization, R_p, is compared with the rate of mass transfer, R_{mt}

$$R_p = \sum_{i=1}^{N} k_p(i) M_c(i) C^*(i) \tag{20}$$

$$R_{mt} = 4\pi r_l(N)^2 k_s [M_b - M_l|_{r_l(N)}] \tag{21}$$

The practical simulations indicated that R_p and R_{mt} were almost equal. This indicates that the QSSA is still valid. Moreover, this solution method requires small time step even later in the particle lifetime otherwise the program will collapse. The reasons for these two cases remain unknown. Moreover, it is obvious that eq. (19) is an appropriate means of discretization when the mass transfer limitations are so severe that QSSA is not valid.

When void fraction is assumed to be constant and to be equal to the original void fraction of the catalyst particle, the mass balance for the macroparticle is simplified into

$$\varepsilon_l \frac{\partial M_l}{\partial t} = D_l\left(\frac{2}{r_l}\frac{\partial M_l}{\partial r_l} + \frac{\partial^2 M_l}{\partial r_l^2}\right) - R_v \qquad (22)$$

The discretization of eq. (22) is similar to that of eq. (11), but the resulting discretization expressions are much more simpler.

The main ideas of the discretization of the energy balance for the macroparticle are similar to those of the mass balance of the macroparticle. The effect of local void fraction on energy transfer is combined in the effective thermal conductivity, k_e, according to Russell's equation.[9] Thus, the discretization of the energy balance requires only one method.

Particle Growth and Grid Updating

Particle growth and grid updating is one of the keys to the solution of the model.

Constant Void Fraction

Procedure 1: Using the volume of the polymer formed in a time step Δt, the positions of the nodes at the time after Δt can be determined roughly by

$$\Delta V_l(j, k) = k_p M_c(j, k) C^*(j, k) V_l(j, 0) \Delta t MW/\rho_p \qquad (23)$$

where MW is the molecular weight of the monomer, ρ_p is the density of the polymer.

$$V_l(j, k+1) = V_l(j, k) + \Delta V_l(j, k) \qquad (24)$$

$$r_l(j, k+1) = \left(\frac{3}{4\pi}\frac{V_l(j, k+1)}{1-\varepsilon_l} + r_l^3(j-1, k+1)\right)^{1/3} \qquad (25)$$

In the above equations, the first term in the parentheses represents the position of some node or layer, while the second one represents the time.

Procedure 2: According to the positions of the nodes at the time after Δt determined in procedure 1, the mass balance for the macroparticle could be solved and the profiles of the monomer concentration, $M_l(j, k+1)$ ($j = 1, 2 \cdots N+1$), could be obtained. The average monomer concentrations in each layer can then be given by

$$M_{l,av}(j, k+1) = \tfrac{1}{2}[M_l(j, k+1) + M_l(j+1, k+1)] \qquad j = 1, 2 \cdots N \qquad (26)$$

Using the equation suitable to describe the sorption of 1,3-butadiene in 1,4-*cis*-polybutadiene, the monomer concentration at the surface of the microparticle, $M_{ss}(j, k+1)$ ($j = 1, 2 \cdots N$), could be yielded.

Procedure 3: Solution of the equations concerning the concentration of the active sites C^*, the microparticle growth factor ϕ_s and the monomer concentration around the active sites M_c

$$C^* = C_0^* k_f M_c\{-\exp[-1/2(\alpha+\beta)t] + \exp[-1/2(\alpha-\beta)t]\}/\beta \qquad (27)$$

where $\alpha = k_d + k_b + k_f M_c$

$$\beta = (k_d^2 + 2k_d k_b - 2k_d k_f M_c + k_b^2 + 2k_f k_b M_c + k_f^2 M_c^2)^{1/2} \qquad (27b)$$

$$M_c = \frac{M_{\text{eq}}(M_l)}{1 + (k_p C^*/3D_s) r_c^2 (R_s - r_c)/R_s} \qquad (28)$$

$$\phi_{s,2} = \left[\phi_{s,1}^3 + \frac{k_p MW(t_2 - t_1)}{\rho_p} \times \frac{[M_c(t_1)C^*(t_1) + M_c(t_2)C^*(t_2)]}{2}\right]^{1/3} \qquad (29)$$

C^* in eq. (27) corresponds to the intrinsic kinetic model of gas phase polymerization of butadiene carried out by Junzi et al.[2] The model emphasized the role of monomer in the formation of active centers from potential centers. The formation of active centers was also reversible.

With the catalytic polymerization whose active site is initiated instantaneously, C^* observes the following expression:

$$C^*(t) = C_0^* \exp(-k_d t) \tag{30}$$

where C_0^* is the concentration of the active sites at time zero, k_d is the constant of deactivation of the active sites, which deactivates at the first order. As for other catalytic system, suitable equation could be obtained according to its intrinsic kinetic model.

Solving eqs. (27)–(30) results in the values of C^*, M_c, and $\phi_s(j, k + 1)$ in each layer.

Procedure 4: When assuming constant void fraction, the positions of the nodes could be determined further in terms of the microparticle growth factor

$$V_l(j, k + 1) = V_l(j, 0)\phi_s^3(j, k + 1) \tag{31}$$

Procedure 5: Apply the node positions determined in procedure 4 to procedure 2. By iteration from procedure 2 to procedure 5, the relevant results could be obtained for the macroparticle and microparticle with accuracy.

The ideas mentioned above are based on increasing calculation precision, but satisfactory results could also be yielded without iteration. Practical simulations, which run directly from procedure 2 to procedure 4 without iteration, indicated that the differences between the two methods are nearly negligible, while the latter can save considerable calculation time.

Procedure 6: The calculations from procedures 1–5 in a time step are based on the assumption that the temperature in the macroparticle is uniform and is equal to the temperature in the reactor. Thus, the profiles of temperature in the macroparticle should be calculated here.

Procedure 7: Using the values of the relevant activation energies and the temperature profile determined in procedure 6, the kinetic constants are determined afresh. Apply the redetermined kinetic constants into the procedure 1. By iteration from procedure 1 to procedure 7, the profiles of monomer concentration and temperature for the macroparticle and the microparticle and other relevant results could be obtained.

Procedure 8: The calculations from procedures 1–7 are made in a time step. Thus, go on to the next time step until the time desired by the reaction.

Variable Void Fraction

As for the case of variable void fraction, the solution method is similar to that of constant void fraction except the determination of the node positions after getting the values of C^*, M_c, and ϕ_s.

Table III Thermal, Physical, and Transport Properties of Gas-Phase Polymerization of Butadiene

Property	Value	Reference
$-\Delta H_p$ (J/mol)	73000	3
C_{pBR} (J/kg K)	1600	3
k_{BR} (W/m K)	0.15	3
ρ_{BR} (kg/m^3)	890	3
C_{pgas} (J/kg K)	1681	3
k_{gas} (W/m K)	0.015–0.021	3
ρ_{gas} (kg/m^3)	4.108–5.4246	3
μ_{gas} (Pa s)	7.8×10^{-6}–8.5×10^{-6}	3
ρ_{cat} (kg/m^3)	623	3
ε_{cat}	0.2–0.4	3, 5, 7
k_e (W/m K)	0.11	9
R_c (μm)	15–100	5
R_s (cm)	10^{-6}–10^{-4}	5
D_b (m^2/s)	2.7×10^{-7}	3
D_l (m^2/s)	10^{-8}–10^{-7}	—
D_s (m^2/s)	1.94×10^{-12}–47.81×10^{-12}	10
u (m/s)	0.02	11

In physical terms, the case of constant void fraction is equivalent to assuming that polymer microparticle, within the macroparticle, rearrange themselves in order to keep the void fraction constant, independent of their relative growth rates. This assumption, which was made by S. Floyd in the original multigrain model in order to simplify calculations, neglects the forces exerted on each microparticle by its immediate neighbors. Hutchinson et al.[7] hold that the spatial arrangement of microparticles within the growing particles does not change; outward shell movement is a result of the pressure exerted by the growing particles within that shell. Thus, if the microparticles in the interior layers of the particle do not grow at a rate sufficient to keep up with those in shell n, an increase in internal void fraction occurs. If the microparticles in the interior shells grow at the same rate as those in shell n, the void fraction within the shell remains constant at its original value, ε_0. Shell position is only dependent on the original shell position and the local growth factor of microparticles within the shell

$$r_l(j, k + 1) = r_l(j, k)\phi_s(j, k + 1) \tag{32}$$

Using the volume balance over shell j from time $k\Delta t$ to time $(k + 1)\Delta t$, the local void fraction, $\varepsilon_l(j, k + 1)$, could be obtained by

$$[r_l^3(j, k + 1) - r_l^3(j - 1, k + 1)][1 - \varepsilon_l(j, k + 1)] = [r_l^3(j, 0) - r_l^3(j - 1, 0)] \times [1 - \varepsilon_l(j, 0)]\phi_s^3(j, k + 1) \quad (33)$$

PARTICLE PARAMETER VALUES

For the gas phase polymerization of butadiene, the range of parameter values one might encounter for polymeric particle, are presented in Table III. The effective thermal conductivity of the polymer particle k_e is calculated using Russell's equation.[9]

ESTIMATION OF TRANSFER PROPERTIES

Diffusivity in Macroparticle

In the polymerization of olefins, it is generally accepted that the diffusion of monomer through the macroparticle is similar to diffusion through a porous catalyst. Diffusivity in the macroparticle for monomer is related to the monomer bulk diffusivity according to

$$D_l = \frac{\varepsilon_l D_b}{\tau} \quad (34)$$

where ε_l is the void fraction of the macroparticle and τ is a tortuosity. τ characterizes the effect of the structure of macroparticle on the macrodiffusion and its value is usually within the range of 2–7; if nothing is known about the structure, a value of 4 is recommended.[7] In this article, this point is adopted to examine the effect of reaction conditions on the void fraction of the macroparticle.

Sorption of Monomer in Polymer Phase

In the polymerization of olefins, Henry's law is generally adopted to describe the sorption of monomer in the polymer phase. Using the critical temperatures of various monomers and inert diluents, their Henry's coefficients can be very well correlated with temperature. However, deviations from Henry's law will occur when the monomer concentration in the polymer phase at sorption equilibrium is high. By contrast, the butadiene molecule, whose volume is comparatively large, will swell 1,4-*cis*-polybutadiene to a comparatively great extent. Thus, Henry's law is not suitable to describe the sorption of 1,3-butadiene in 1,4-*cis*-polybutadiene. In this article, the Flory–Huggins thermal is adopted according to TongBa's experimental results[10]:

$$S = \frac{M_{ss}}{p} = k_D e^{\delta M_{ss}} \quad (35)$$

where p is the partial pressure of monomer in the interstices between the microparticles, k_D and δ are parameters whose values are dependent on temperature. Solving nonlinear eq. (35) results in the monomer concentration at the surface of the microparticles M_{ss}, i.e., $M_{eq}(M_l)$.

Diffusivity in Microparticle

TongBa[10] conducted studies on the diffusion of 1,3-butadiene through a compact film made of 1,4-*cis*-polybutadiene and obtained the following conclusion:

$$D_s = D_{s0} e^{\gamma c} \quad (36)$$

where D_{s0} and γ are parameters whose values are dependent on temperature and monomer pressure. Because eq. (36) could be used to describe the effect of temperature and pressure on the diffusivity in the microparticle, this article examines the effect of reaction conditions on diffusivity in the microparticle.

Heat and Mass Transfers at the Polymer Particle Boundary Layer

The effects of mass and heat transfers at the external boundary layer of the polymeric particle have been considered, using the Ranz–Marshall correlation for the heat and mass transfer coefficients[11]

$$Nu = 2 + 0.6Re^{1/2}Pr^{1/3} \quad (37)$$

$$Sh = 2 + 0.6Sc^{1/3}Re^{1/2} \quad (38)$$

where Nu is the Nusselt number, hd_p/k_f, Re is the Reynold's number, $\rho_d u d_p/\mu_f$, Pr is the Prandt number, $\mu C_{pf}/k_f$, Sh is the Sherwood number, $k_s d_p/D_b$, and Sc is the Schmidt number, $\mu/\rho_d D_b$.

CONCLUSIONS

In this article, some improvements to the multigrain model were made in order to simulate the growth and morphology of polymeric particle in the gas phase polymerization of butadiene. In the model, the effects of heat and mass transfers, sorption of monomer in the polymer phase, intrinsic kinetics on growth and morphology of polymer particle were considered reasonably. An improved numerical solution technique was also proposed. The discretization of the model equations and grid updating were the keys to the solution of the model.

NOMENCLATURE

C^*	concentration of active sites, molsite m^{-3} cat or mol site g^{-1} cat
C_0^*	concentration of active sites at time zero, mol site m^{-3} cat or mol site g^{-1} cat
C_p	heat capacity of polymer, J kg^{-1} K^{-1}
C_{pBR}	heat capacity of 1,4-*cis*-polybutadiene, J kg^{-1} K^{-1}
C_{pf}	heat capacity of monomer gas, J kg^{-1} K^{-1}
$C_{p\text{gas}}$	heat capacity of monomer gas, J kg^{-1} K^{-1}
D_b	bulk diffusivity of monomer, cm^2 s^{-1}
D_l	effective diffusivity in the macroparticle, cm^2 s^{-1}
D_s	effective diffusivity in the microparticle, cm^2 s^{-1}
D_{s0}	diffusivity when concentration approaches zero, cm^2 s^{-1}
d_p	diameter of the polymer particle, m
E_A	activation energy for propagation, kJ mol^{-1}
$-\Delta H_p$	heat of polymerization, J mol^{-1}
h	external film heat transfer coefficient, W m^{-2} K^{-1}
k_b	rate constant of the deformation of active centers, s^{-1}
k_{BR}	thermal conductivity of BR, W m^{-1} K^{-1}
k_D	sorption coefficient when concentration approaches zero, L(STP) L polymer^{-1} Pa^{-1}
k_d	rate constant of deactivation of the active site, s^{-1}
k_e	effective thermal conductivity of polymer particle, W m^{-1} K^{-1}
k_f	rate constant of the formation of active centers, L polymer mol^{-1} s^{-1}
k_f	thermal conductivity of monomer gas, W m^{-1} K^{-1}
k_p	propagation rate constant, L polymer mol site^{-1} s^{-1}
k_s	external film mass transfer coefficient, m s^{-1}
M_b	bulk monomer concentration, mol L^{-1}
M_c	monomer concentration at catalyst surface, mol L polymer^{-1}
$M_{\text{eq}}(M_l)$ or M_{ss}	monomer concentration at surface of microparticle, mol L polymer^{-1}
$M_l(r_l, t)$	monomer concentration in pores of macroparticle, mol L^{-1}
$M_{l,\text{av}}$	average monomer concentration in shells of macroparticle, mol L^{-1}
M_{ls}	monomer concentration at macroparticle surface, mol L^{-1}
$M_s(r_s, t)$	monomer concentration in microparticle, mol L polymer^{-1}
MW	molecular weight of monomer
Nu	Nusselt number, $Nu = hd_p/k_f$
Pr	Prandt number, $P_r = \mu C_{pf}/k_f$
R_c	radius of catalyst particle, m
R_{cs}	rate of polymerization at catalyst particle surface
Re	Reynolds number, $Re = \rho_d u d_p/\mu_f$
R_l	radius of macroparticle, m
R_p	overall polymerization rate, g BD g cat^{-1} h^{-1}
R_s	radius of microparticle, m
R_v	volumetric reaction rate in the macroparticle
r_{crys}	catalyst primary crystallite radius, m
r_l	macroparticle radius, m
$r_l(j, k)$	position of node j at time k, m
r_s	microparticle radius, m
Sc	Schmidt number, $Sc = \mu/\rho_d D_b$
Sh	Sherwood number, $Sh = k_s d_p/D_b$
T_b	temperature in the reactor, K
$T_l(r_l, t)$	temperature in the macroparticle, K

$T_s(r_s, t)$	temperature in the microparticle, K
t_l, l_2	time of discretization, s
Δt	time step, s
u	particle–fluid relative velocity, m s^{-1}
V_s	volume of microparticle, m^3
V	volume of polymer and catalyst in each shell, m^3
ΔV	volume of polymer formed during one time step, m^3

GREEK SYMBOLS

α_s	Thiele modulus
ε_{cat}	void fraction of catalyst particle
ε_l or $\varepsilon_l(r_l, t)$	void fraction of macroparticle
μ_f	viscosity of fluid, Pa · s
μ_{gas}	viscosity of monomer gas, Pa · s
ρ_{BR}	density of polymer, kg m^{-3}
ρ_{cat}	density of catalyst particle, kg m^{-3}
ρ_{gas}	density of monomer gas, kg m^{-3}
ρ_p	density of polymer, kg m^{-3}
τ_{M_s}	time constant for concentration equilibrium, s
τ_{T_s}	time constant for temperature equilibrium, s
ϕ_s	microparticle growth factor

REFERENCES

1. Eberstein, C.; Garmatter, B.; Reichert, K. H.; Sylvester, G. Chem Ingen Technik 1996, 68, 820.
2. Junzi, Z.; Jianzhong, S.; Qiyun, Z.; Zuren, P. J Chem Ind Eng (China), to appear.
3. Jianzhong, S.; Eberstein, C.; Reichert, K. H. J Appl Polym Sci 1997, 64, 203.
4. Soares, J. B.; Hamielec, A. E. Polym React Eng 1995, 3, 261.
5. Floyd, S.; Choi, K. Y.; Taylor, T. W.; Ray, W. H. J Appl Polym Sci 1986, 32, 2935.
6. Floyd, S.; Heiskanen, T.; Taylor, T. W. J Appl Polym Sci 1987, 33, 1021.
7. Hutchinson, R. A.; Chen, C. M.; Ray, W. H. J Appl Polym Sci 1992, 44, 1389.
8. Garmatter, B. M.S. Thesis, Technical University of Berlin, Berlin, 1995.
9. Perry, R. H.; Chilton, C. H., Eds. Chemical Engineering's Handbook; 5th Ed.; McGraw-Hill: New York, 1982.
10. TongBa, H. M.S. Thesis, Technical University of Berlin, Berlin, 1995.
11. Floyd, S.; Choi, K. Y.; Taylor, T. W.; Ray, W. H. J Appl Polym Sci 1986, 31, 2231.